



A configurational force-based material point method for crack propagation modelling in 2D

Rongxin Zhou^{a,*}, William M. Coombs^b, Yang Xu^c, Ping Zhang^d, Li-Ge Wang^{e,f}

^a School of Civil Engineering, Hefei University of Technology, 230009, China

^b Department of Engineering, Durham University, DH1 3LE, UK

^c School of Mechanical Engineering, Hefei University of Technology, 230009, China

^d School of Power and Energy, Northwestern Polytechnical University, Xi'an 710129, China

^e Department of Chemical and Biological Engineering, University of Sheffield, UK

^f Process Systems Enterprise, Hammersmith, London, UK

ARTICLE INFO

Keywords:

Material point method
Configurational force
Fracture mechanics
Crack propagation

ABSTRACT

The modelling of fracture initiation and propagation is a nontrivial problem in computational mechanics. However, it is an area that is extremely important in engineering applications, requiring accurate and robust numerical methods that can be applied to a variety of materials. This paper presents the development of a new numerical modelling approach, which combines material, or configurational, forces and the material point method (MPM), for finite deformation crack modelling of linear elastic solids in two dimensions. The combination of these numerical methods offers a number of advantages relating to the flexibility of the MPM in terms of decoupling the material deformation from the computational grid and the general nature of configurational force theory in terms of being applicable across different material behaviour. In the method presented in this paper, the MPM forms the basis of the mechanical response of the underlying material, while the configurational force theory provides a fracture criterion for crack modelling through a post-processing procedure. The developed modelling framework is applied to a number of benchmark problems for linear elastic solids in 2D. All simulations show good agreement with the results in the literature, which demonstrates that the combined configuration force-material point framework is a promising numerical tool for fracture modelling.

1. Introduction

Failure of engineering structures is usually accompanied by cracking of solid materials, which is strongly affected by geometrical characteristics and material properties of specimens as well as the loading conditions. Therefore, crack modelling in solid materials is of great importance, both in terms of understanding fracture behaviour and in ensuring the safety of engineering structures [1]. However, there are a number of numerical challenges that manifest themselves when modelling fracture mechanics problems linked to the numerical platform adopted for stress analysis and the selected crack propagation criteria. Generally, computation modelling of fracture in solid materials can be classified into three categories, namely: continuum-based approaches, block-based methods and discrete crack approaches [2].

Continuum-based approaches e.g. smeared crack methods are widely used in engineering problems due to their easy implementation into

commercial software [3]. These approaches introduce a characteristic length scale and spread the discrete crack over a finite-sized domain [4]. No real cracks are modelled, instead, crack opening and crack sliding are replaced by crack strain [5], and the stiffness degradation process around the fractures is represented by strain softening. These methods are good candidates when global responses are of interest but not suitable for applications where detailed information around a crack tip is of interest [6]. Previous research has also shown some long-standing problems, such as mesh-size dependency, and limited deformation modes of standard continuum elements when modelling softening behaviour [5,7,8]. Nonlocal [e.g. [9,10]] and gradient approaches [e.g. [11–13]] have been proposed successfully to remedy the severe mesh sensitivity that results from the introduction of strain-softening, but some open issues persist such as the determination of the additional material parameters and the physical nature of the additional boundary conditions required for such methods [5].

* Corresponding author.

E-mail address: rongxinzhou@hfut.edu.cn (R. Zhou).

<https://doi.org/10.1016/j.tafmec.2021.103186>

Received 8 July 2021; Received in revised form 12 November 2021; Accepted 15 November 2021

Available online 18 November 2021

0167-8442/© 2021 The Authors. Published by Elsevier Ltd. This is an open access article under the CC BY license (<http://creativecommons.org/licenses/by/4.0/>).

The Block-Based Methods (BBMs) model the material or structure through interaction/contact of an assembly of blocks and the most popular block-based method is the Discrete Element Method (DEM) [14]. The main principle behind this approach is to bound an assembly of blocks to each other using cohesion at the contact surfaces between adjacent blocks [2]. The BBM possess inherent advantages in accommodating crack-induced discontinuities. However, the method's ability to model continuum and partially damaged phases of solid materials is dependent on the equivalent description of the continuum properties through contact surfaces, which is difficult to generalize for different stress conditions [15]. In addition, the computational cost of these methods is high as a large number of underlying block interactions are required to be resolved during each calculation step.

Discrete cracks can be modelled within the Finite Element Method (FEM) by introducing cohesive interface elements between adjacent elements [16–18]. However, these methods can only allow cracks to develop along existing inter-element edges, which makes the simulation results depend not only on the mesh size but also on the mesh bias [18]. An alternative is the Embedded Finite Element Method (EFEM) or the eXtended Finite Element Method (XFEM), in which knowledge about the solution around the fractures is introduced into the solution field and additional degrees of freedoms are condensed at an element or nodal level. The enrichment of the displacement field in these methods allows displacement jump within elements to be captured and crack propagation is possible without remeshing [19,20]. However, it has been reported in the literature that EFEM and XFEM are only suitable for problems with a few number of cracks [2]. For complex fracture patterns, they may introduce some inaccuracies including stress locking, violation of traction continuity and/or potential inaccuracies in the representation of the displacement field [21].

More recently, advanced numerical approaches, for example, phase-field [22,23] and thick level set [22,23] approaches are also used for crack propagation modelling. The advantage of these approaches is that it is not necessary to track the complex evolution cracking surface, making them much more suitable for complex fracture patterns such as crack branching, coalescence, deflection and nucleation, especially in 3D problems.

The meshfree methods are also suitable for discrete crack modelling due to the absence of a mesh and depending on the target application, different approaches in the meshfree methods can be adopted. A simple and efficient method to deal with fractures in the meshfree methods is the Cracking Particles Method (CPM) [24–26]. The CPM treats the crack as a set of crack segments and does not require crack path continuity. Therefore, it is particularly useful for complex crack patterns such as branched cracks. Recently, a novel non-local extension form of continuum mechanics, called Peri Dynamics (PD) [27], has been attractive to researchers for crack modelling. Unlike classical approaches incorporating partial derivatives, PD utilises integral expressions in the governing equations such that cracks and any other discontinuities in materials and structures can be treated naturally without special techniques [28,29]. However, this method is still in its infancy and several challenges remain, e.g. incorporating complex constitutive models and verification towards experimental results [30]. In addition, the vast majority of PD formulations require a uniform discretization and have non-local support which leads to high computational cost [31].

Another effective and simple semi-meshfree method to model fracture is the Material Point Method (MPM) [32]. MPM has been found to offer significant computational advantages when compared with purely meshless methods since it does not require time-consuming neighbour searching [33]. The main difference between MPM and meshfree particle methods (e.g. SPH, EFG) is that in MPM, the equations of motion are solved on the background grid and material points are used as the quadrature points to approximate nodal forces and nodal masses, while in the meshfree methods the equations of motion are solved on the meshfree points and a background mesh is often constructed to integrate the governing equations. MPM has potential advantages over FEM for

modelling of crack propagation because there is no need for cracks to follow grid lines. In MPM, the background grid is only used as a tool to solve the equations of motion, and not used to describe the object or the crack [34]. In other words, the crack is not constrained by grid lines and is free to be oriented and to propagate in any direction as the background mesh can be redefined to coincide with the appropriate crack propagation path. Additional advantages of MPM in solving the crack propagation compared with FEM include that the sharp discontinuities in the displacement field can be naturally treated, as the response is monitored at material points that move within a background Eulerian grid [35]. Thus, no re-meshing or enrichment of the underlying finite element mesh is required when cracks propagate as the latter is relieved from the detrimental effects of mesh distortion. The MPM also naturally handles history-dependent material behaviour, such as elastoplasticity or damage, without remapping of state variables when the background mesh is adapted as the state variables *live* at the material points. This is not the case with the standard FEM where the integration points are intimately tied to their parent element, and when the mesh is adapted the state variables of the old parent element need to be mapped to the new parent element. Successful implementation of MPM for crack propagation can be found in the published literature [e.g. [36–38]]. In these studies, contact and cohesion mechanisms have been used and crack propagations are treated as decohesion between neighbour material points. However, this kind of fracture simulation is computationally expensive and prohibitive for large scale simulations. In the present study, a simpler method in which cracks are introduced in the background grid is adopted. Crack propagation is achieved by a stepwise release of segments of the background computational grids at a prescribed load.

The challenge of modelling fractures in engineering materials also relies on a suitable fracture criterion. The fracture criteria in numerical modelling are used to determine whether or not a crack will propagate or nucleate. Moreover, appropriate fracture criteria should provide the orientation and the 'length' of crack propagations [3]. In numerical simulations, the prediction of the crack propagation direction has a significant effect on the modelling results, as a small perturbation in the crack propagation direction can result in a completely different crack pattern and global force–displacement response. Several crack propagation criteria have been proposed, e.g. critical stress intensity factor K , the energy release rate G , the crack tip opening displacement CTOD, etc. However, each criterion has associated issues. The critical stress intensity factor approach is only suitable for problems with small-yielding assumptions [39]. The CTOD criteria have the limitation that it is not suitable for predicting the crack deflection or kinking from the original crack direction under mixed-mode loading conditions [40]. In addition, it is difficult to determine experimentally as measurements are required to be taken in the interior of a specimen [41].

In addition to selecting a crack propagation direction criterion, numerical modelling approaches also require a method to determine the crack tip information that can be used to determine if a crack will propagate. The J -integral possesses the computationally attractive property of integration-path independence and is widely used on problems without material inhomogeneities [42]. However, the J -integral approach presumes deformation plasticity and treats elastic–plastic material as non-linear elastic. For a growing crack in a real elastoplastic material, the J -integral based on deformation plasticity assumption loses its role as a crack driving force [43]. Moreover, the definition of J -integration restricts its application to cases of monotonic loading. An alternative is to use fracture criteria based on configurational force theory, which was first proposed by Eshelby [44], has been successfully used for crack propagation in numerical simulations [42]. According to its definition, the configurational force can be considered as the thermodynamic force which is responsible for the motion of cracks in materials. One of the advantages of using the configurational force approach is that it can be adapted to all kinds of material models [43] (elastic, finite elastic, visco-elastic, plastic, coupled mechanics, etc.)

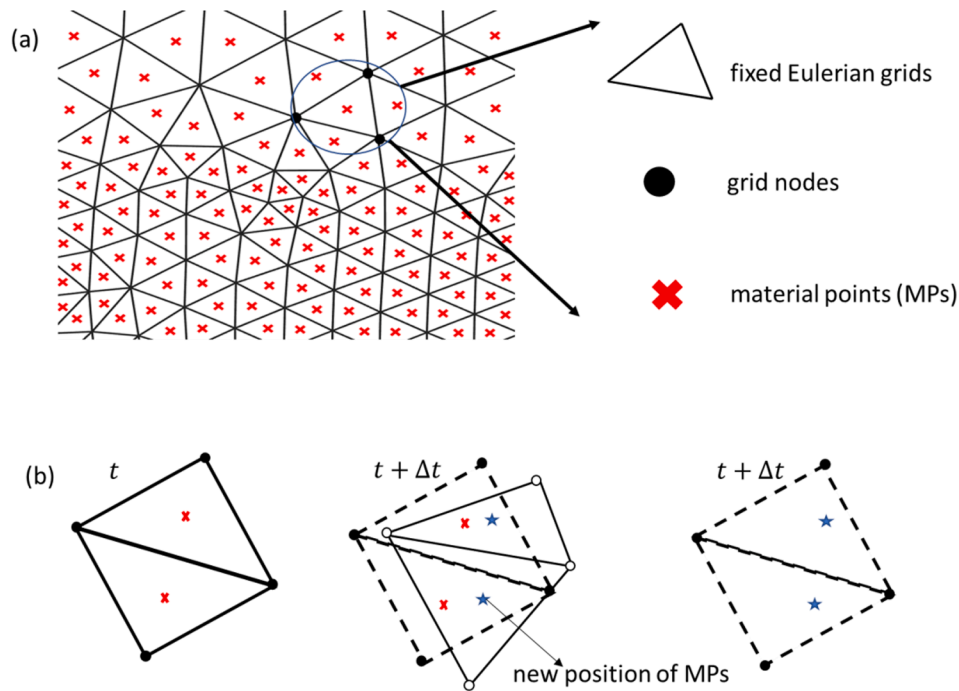


Fig. 1. Sketch of material point method: (a) discretization of material domain; (b) moving material points through background mesh.

without making any assumptions. Applications of this method can be found in brittle crack modelling [45,46], elastoplastic materials [42,43], 3D cracks [1,47], dislocations [48,49], crystal plasticity [50] and crack branching in dynamics [51]. However, most of these studies were limited only to the finite element framework. The implementation of this criterion into more advanced numerical approaches, such as MPM, is very rare in the literature.

This paper presents an implementation of the configurational force theory for crack propagation modelling in an MPM framework. MPM forms the basis of the mechanical model while the configurational force theory provides a fracture criterion for the crack propagation. To the best of the authors' knowledge, this is the first time that the configurational force criterion has been combined with an MPM framework. The combination of these two approaches provides a powerful framework for modelling fracture in general materials. However, this paper is focused on linear elastic materials within a large deformation framework to provide the essential basis for future extensions.

2. Material point method

The MPM has received increased traction in commercial applications in recent years due to its outstanding performances in large deformations [52–54] as well as crack propagation [35]. The method uses two discretizations of the material domain. One is based on a computational grid and the other one is based on a collection of material points. Fig. 1(a) shows a graphical illustration of the discretization in MPM. The background grid is used to determine incremental displacements by solving the governing equations while all the material state variables including stress, strain, history-dependent plastic information, are carried by material points. The deformation of the material is modelled by moving material points through the mesh. At each time step, the obtained displacements from grid nodes are transferred back to the corresponding material points such that all material state variables can be updated accordingly. At this point, MPM is identical to FEM in which the material points are served as integration points and the background grid serves as a finite element mesh. However, in MPM the deformed background grid is discarded i.e., it is reset to the initial configuration (undeformed) after each time step. This is the distinctive advantage of MPM

over FEM and makes this method ideal for modelling large deformation problems while avoiding mesh distortion [52–54]. Fig. 1(b) presents general steps of the deformation process in the MPM.

MPM can be considered as the updated Lagrangian finite element method in which material points perform as integration points but are uncoupled from the background computational grid. From the authors' perspective, the key difference between the FEM and MPM is that these integration points move accordingly with the background grid rather than being directly coupled to the position of the computational grid nodes. Therefore, it is necessary to track the movement of the material points and to know the computational grids that they belong to at each time step.

2.1. Updated Lagrangian mechanics

In this section, a quasi-static implicit finite deformation MPM based on an updated Lagrangian formulation is presented. The weak statement of equilibrium is expressed as

$$\int_{\varphi_t(\Omega)} (\sigma_{ij}(\nabla_x \eta)_{ij} - b_i \eta_i) dv - \int_{\varphi_t(\partial\Omega)} (t_i \eta_i) ds = 0, \quad (1)$$

where φ_t is the motion of the material body with domain, Ω , which is subjected to tractions, t_b , on the boundary of the domain (with the surface, s), $\partial\Omega$, and body force, b_i , acting over the volume, v , of the domain. These external loads lead to a Cauchy stress field, σ_{ij} , through the body. The weak form is expressed in the current frame with the assumption of a field of admissible virtual displacements, η_i . However, MPMs are unusual in that they are not ideally suited to the traditional total or updated Lagrangian formulations of continuum mechanics [51]. This is due to the fact that their basis functions are normally based on material point positions at the start of a load step and assume that calculations take place on the undeformed grid. This means that care must be taken when implementing an updated Lagrangian material point method in terms of the spatial derivatives of the basis functions to ensure that they correctly satisfy the weak form of the governing equations [52]. The formulation present in this section is essentially the same as that used in [52] and available in the open-source AMPLE code [55].

A combination of logarithmic strain with Kirchhoff stress is used in

the present study to allow the use of conventional small strain constitutive models within a finite deformation framework. This formulation is one of the most straightforward ways to implement large strain within a finite element framework [54]. At each material point, stress and strain are expressed with an exponential map of the plastic flow equation so that the stress integration algorithm used in the plasticity model can be the same with a small strain problem. Although linear elastic solids are considered in the present study only, the extension of the current code to elastoplasticity is straightforward and will be reported in a separate paper. In order to obtain the updated stress state for the current deformation gradient, the adopted constitutive model requires trial stress to act as the elastic strain state. In this approach, the trial elastic Cauchy-Green strain and logarithmic strain is obtained from

$$(b_t^e)_{ij} = \Delta F_{ik}(b_n^e)_{kl}\Delta F_{jl}, \text{ and } (\epsilon_t^e)_{ij} = \frac{1}{2} \ln(b_t^e)_{ij}, \quad (2)$$

where ΔF_{ik} is the increment in the deformation gradient over the current load step and the subscript t and n denote trial and previously converged states, respectively.

2.2. Discrete material point formulation

By introducing the element approximation for the displacements at a point within a finite element, the Galerkin form of the weak statement of equilibrium over one element in the background mesh, E , can be obtained as

$$\{f_E^R\} = \int_{\varphi_t(E)} [\nabla_x S_{vp}]^T \{\sigma\} dv - \int_{\varphi_t(E)} [S_{vp}]^T \{b\} dv - \int_{\varphi_t(\partial E)} [S_{vp}]^T \{t\} ds = \{0\}, \quad (3)$$

where $[\nabla_x S_{vp}]$ is the strain–displacement matrix containing derivatives of the basis (or shape) functions that link the material points (subscript p) with the nodes or vertices of the background grid (subscript v) with respect to the updated coordinates, and $[S_{vp}]$ is the matrix form of the basis functions. In order to keep the implementation similar to FEM as much as possible, the same basis functions in FEM are also used in the present study for MPM. The basis functions and their spatial derivatives for the standard MPM are

$$S_{vp} = S_v(\{x_p\}) \text{ and } \nabla S_{vp} = \nabla S_v(\{x_p\}), \quad (4)$$

where S_v is the standard FEM basis function of the node v and x_p are the coordinates of material point p . The internal force within one element is approximated in the first term in Eq. (3) while the external force vector is combined by the second term (body forces) and the third term (tractions).

In MPM the physical domain is discretised by a number of material points, it is more convenient to express the global equilibrium Eq. (3) in terms of material point contribution, rather than element, contribution.

In this context, the global residual vector, $\{f^R\}$, can be assembled through

$$\{f^R\} = \{f^{int}\} - \{f^{ext}\}, \quad (5)$$

where $\{f^{int}\}$ and $\{f^{ext}\}$ are the global internal and external force vectors. They can be respectively obtained as

$$\{f^{int}\} = \prod_{\forall P} \left\{ [\nabla_x S_{vp}]^T \{\sigma\} V_p \right\}, \quad \{f^{ext}\} = \prod_{\forall P} \left([S_{vp}]^T \{b\} V_p \right) + \int_{\varphi_t(\partial E)} [S_{vp}]^T \{t\} ds, \quad (6)$$

where V_p is the current volume associated with the material point and \prod is the standard assembly operator. For the standard MPM which is adopted in the present study, the V_p is updated after each load step through

$$V_p = \det(F_{ij})V_p^0 = \det(\Delta F_{ij})V_p^n, \quad (7)$$

where V_p^0 and V_p^n are the volumes associated with the material point in the initial configuration and the previously converged state, and n denotes the load step number. Within the discrete formulation of the MPM, the increment of the deformation gradient, ΔF_{ij} in Eq. (7) can be obtained from the derivatives of the basis functions based on the configuration at the start of the load step:

$$\Delta F_{ij} = \delta_{ij} + \frac{\partial \Delta u_i}{\partial \bar{X}_j} = \delta_{ij} + \sum_{v=1}^N (\Delta u_v)_i \left\{ \frac{\partial S_{vp}}{\partial \bar{X}_j} \right\}^T, \quad (8)$$

where Δu_v is the displacement increment of a background grid node v within the current load step and N is the number of nodes that influence the material point. Eq. (8) allows the determination of the increment in the deformation gradient based on the initial (undeformed) computational grid. However, in order to calculate the internal force in Eq. (6), it is necessary to obtain the derivatives of the shape functions with respect to the current coordinate, x_i , consistent with the updated Lagrangian formulation [52]. According to the chain rule, the spatial derivative of the basis functions can be calculated as [52]

$$\frac{\partial S_{vp}}{\partial x_j} = \frac{\partial S_{vp}}{\partial \bar{X}_i} \frac{\partial \bar{X}_i}{\partial x_j} = \frac{\partial S_{vp}}{\partial \bar{X}_i} (\Delta F_{ij})^{-1}. \quad (9)$$

Assuming that the applied body force and surface tractions are independent of the nodal displacement, the global stiffness matrix, $[K]$, can then be obtained by linearizing the internal force in Eq. (6) as

$$[K] = \prod_{\forall P} \left\{ [\nabla_x S_{vp}]^T [a] [\nabla_x S_{vp}] V_p \right\}. \quad (10)$$

Here, $[a]$ is spatial consistent tangent modulus matrix for a material point and can be given by

$$a_{ijkl} = \frac{1}{2J} D_{ijmn}^{alg} L_{mnpq} B_{pqkl} - T_{ijkl}, \quad (11)$$

where

$$L_{mnpq} = \frac{\partial \ln(b_{mn}^e)}{\partial b_{pq}^e}, \quad B_{pqkl} = \delta_{pk} b_{ql}^e + \delta_{ql} b_{pk}^e, \quad T_{ijkl} = \sigma_{ij} \delta_{jk}, \quad (12)$$

and D_{ijmn}^{alg} is the small-strain algorithm tangent obtained from the constitutive model. The use of this tangent allows for asymptotic quadratic convergence of the global residual in Eq. (5), see details in [56].

Eq. (5) is non-linear in terms of the unknown nodal displacements and can be efficiently solved using the standard Newton-Raphson (NR) procedure. The nodal displacement increments within a load step, $\{\Delta d\}$, can be obtained by iteratively updating the nodal displacement increments until Eq. (5) is satisfied within a given tolerance using

$$\{\delta d\}_{k+1} = [K]^{-1} \{f^R\}_k, \quad (13)$$

where $k + 1$ denotes the current iteration number, $\{\delta d\}_{k+1}$ are the iterative nodal displacements, $\{f^R\}_k$ is the global residual out-of-balance vector in Eq. (5) from the k th iteration. The displacement increments in a load step then can be obtained by summing the iterative increments within the load step, that is $\{\Delta d\} = \sum_{it=1}^{k+1} \{\delta d\}_{it}$, where it refers to the iteration number.

Once equilibrium has been obtained, the material point positions and volumes should be updated. The positions of material points are updated through

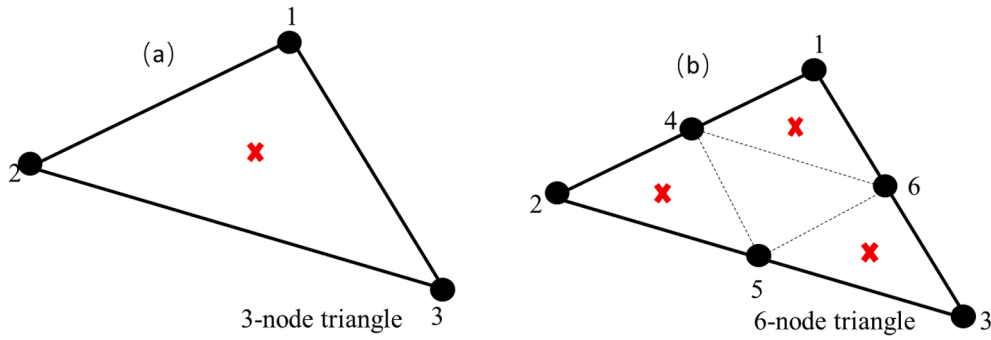


Fig. 2. Triangle elements and initial material point distribution: (a) 3-node element; (b) 6-node element.

$$(x_p)_i = (\tilde{X}_p)_i + (\Delta u_p)_i = (\tilde{X}_p)_i + \sum_{v=1}^N S_{vp}(\Delta u_v)_i, \quad (14)$$

where $(\Delta u_p)_i$ and $(\Delta u_v)_i$ are the displacement increments for material point and the corresponding background mesh grid node, respectively. The volume at each material point, as discussed above, can be updated through Eq. (7).

2.3. Background mesh and basis functions

Most MPM implementations adopted a uniform Cartesian grid which consists of lines in 1D, squares in 2D and cubes in 3D. However, some implementations utilizing an unstructured mesh as the background computational grid. In the present study, triangular background computational grids are preferred so that the detailed crack paths could be simulated more realistically [18]. However, it should be noted that contrary to the Cartesian grid, the search for which computational grid contains a given material point can be a challenge in an unstructured mesh. In this study, a subroutine based on checking the relative position of material points for all the computational triangle grids is developed to solve this problem. The algorithm is based on checking the number of points in the convex hull of the vertices of the triangle adjoined with the material point in question. If the hull has three vertices, the material point lies in the triangle's interior; if it is four, it lies outside the triangle.

In this paper, two triangle elements, namely 3-node and 6-node (see Fig. 2) are used to discrete the background space. As stated earlier, the same basis functions in a local coordinate system used in FEM are adopted in MPM in the present study. The use of local coordinate systems makes the derivation of the shape functions much easier and they are common across all background elements.

Unlike the Gauss integration points in traditional FEM, the relative position of a material point within an individual background grid keeps moving during the loading process. Therefore, it is not necessary to couple the initial material point position with the background computational grid in MPM. One can freely distribute material points within the material domain, especially for the case with structured background meshes. In the present study, to simplify the procedure but without loss of accuracy [57], only one MP within the 3-node computational grid is considered and its initial position is located at the centre of the triangle (see Fig. 2(a)) while three MPs within the 6-node triangle are considered and they are initially located at the centre of small triangles $\Delta 146$, $\Delta 426$ and $\Delta 653$, respectively, as shown in Fig. 2(b). Understandingly, 6-node triangles will increase the computational cost when solving crack propagation problems.

3. Configurational force theory

3.1. Concept of configurational force

The general theory of configurational force mechanics can be traced

back to the work of Eshelby [44], in which it is defined as a generalized force acting on ‘defects’ such as inclusion, vacancy, dislocation, crack and so on. The variation of the free energy associated with a variation of the configuration defines a configurational force (CF), which, in its turn, drives the configuration change of the structure [58]. Contrary to physical forces, configurational forces (CF) act on the material space and it generally can be interpreted as the representation of the negative gradient of the strain energy function with respect to the position of a ‘defect’ [44]:

$$CF_i = - \frac{\partial \psi(\alpha, X)}{\partial X_i}, \quad (15)$$

where ψ refers to the total energy and it can be written as a function of several quantities, α_i , and the position in the material space, X_i .

Following the work by Esheby in [44], the energy change associated with an infinitesimal movement of the ‘defect’, $\delta \xi$, can be expressed as

$$\delta \psi = - \delta \xi_i \int_{\Gamma} \Sigma_{ij} n_j d\Gamma, \quad (16)$$

in which n_j is the outward unit normal to the surface of the ‘defect’, Γ , and Σ_{ij} is the Eshelby stress tensor. Considering the energy change, $\delta \psi$, as a scalar product of the configurational force CF_i with the infinitesimal displacement, $\delta \xi_i$, Eq. (16) can be recast into the form:

$$\delta \psi = \delta \xi_i (CF)_i. \quad (17)$$

The configurational force, CF_i is obtained correspondingly, as

$$CF_i = - \int_{\Gamma} \Sigma_{ij} n_j d\Gamma, \quad (18)$$

In the present study, constitutive models adopt a fully implicit stress integration algorithm. Therefore, although the framework is for finite deformation problems, the deformation within each step can be still considered to small. Then the Eshelby stress tensor is defined as

$$\Sigma_{ij} = \psi \delta_{ik} - u_{j,i} \sigma_{jk}, \quad (19)$$

where ψ is the internal strain energy of the solid,

$$\psi = \frac{1}{2} \sigma_{ij} u_{ij}, \quad (20)$$

$u_{i,j}$ is the gradient of the displacement field. Considering a closed-form ‘defect’, Eq. (18) can be converted to a domain integral using Green’s theorem, as

$$CF_i = - \int_{\Gamma} \Sigma_{ij} n_j d\Gamma = - \int_{\Omega_c} (\Sigma_{ji,j}) d\Omega_c, \quad (21)$$

in which Ω_c is the domain of the ‘defect’ encircled by the contour Γ . Eq. (21) indicates that the configurational force at a position is determined by the divergence of the configurational stress in a region around the point – parallels can be drawn between this and the conventional

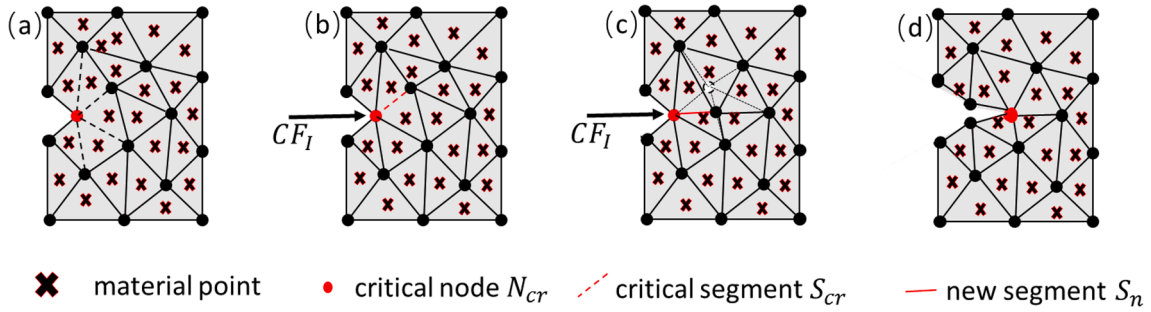


Fig. 3. Crack propagation procedure in MPM framework: (a) identification of the critical node and its corresponding segments; (b) identification of the critical segments according to the configurational force vector CF_I ; (c) Alignment of the critical segment in direction of the configurational force CF_I and node doubling; (d) crack propagation through segment release.

definition of the internal force at a node via integration of the Cauchy stress in the elements attached to a node.

For linear elastic materials, the strain energy may be expressed as

$$\psi = \psi(\varepsilon_{ij}, X_i) \quad (22)$$

and is only dependent on the strain ε_{ij} and the position of the material point X . Therefore, the gradient of the assumed strain energy yields:

$$\nabla\psi = \nabla\psi(\varepsilon_{ij}, X_i) = \sigma_{jk}u_{ji,k} - (\psi\delta_{ik})_{,k}, \quad (23)$$

where $(\psi\delta_{ik})_{,k}$ denotes the explicit dependence of ψ on position X . Additionally, using differentiation by part on $\sigma_{ij}\nabla\psi(\varepsilon_{ij})$, a local energy momentum balance can be obtained as

$$\nabla \cdot (\Sigma_{ij}) = 0, \quad (24)$$

in which Σ_{ij} is the Eshelby stress tensor defined in Eq. (19). Integrating Eq. (24) over a simply connected domain and using Green's divergence theorem, the resultant of the Eshelby stress for a contour path Γ encircling a closed-form domain must vanish, as

$$\oint_{\Gamma} \Sigma_{ij}n_j d\Gamma = 0, \quad (25)$$

where n_j is the outward normal to Γ . For the problem domain containing defects or cracks, as is the case in the present study, if boundaries of the specimen and crack surfaces are included to form a closed-form, the balance of energy momentum can be still achieved [41,59,60], i.e. the resultant from Eq. (24) and (25) is zero.

3.2. Implementation of configurational force in the MPM

Numerical implementation of configurational force as the crack driving force in the FEM framework for elastic solids can be found in the work of Miehe et al. [45,46] and Denzer et al. [61]. Miehe et al. [46] gave an expression of the configurational force at the crack tip, CF^{tip} ,

$$CF^{tip} = - \prod_{e=1}^{aelem} \int_{\Omega^e} \Sigma_{ij} \frac{\partial S_{vp}}{\partial X_j} d\Omega, \quad (26)$$

where $aelem$ is the number of elements attached to the crack-tip node. However, a more accurate form based on a domain surrounding the crack tip is proposed by Denzer et al. [61]

$$CF^{domain} = - \sum_{N=1}^{N_{np}} \prod_{e=1}^{N_{elem}} \int_{\Omega^e} \Sigma_{ij} \frac{\partial S_{vp}}{\partial X_j} d\Omega, \quad (27)$$

where the crack driving force can be deemed as the resultant of all configurational force vectors in elements over the specific domain Ω , surrounding the crack tip in the numerical evaluation. In Eq. (27), N_{np} and N_{elem} refer to the number of nodes and elements within the specified

domain Ω , respectively.

As stated in previous sections, MPM and FEM share several common aspects and the material points can be considered as moving integration points in FEM. Therefore, the method proposed by Denzer et al. [61] can be used in the present MPM framework without much additional effort. The stress and displacement fields are still calculated and updated within the MPM framework, following the algorithm stated in Section 2. The CF is calculated through a post-processing procedure on the nodes of the background grids.

4. Crack propagation and computational framework

4.1. Algorithm for crack propagation in elastic solids

In the present study, the crack propagation is assumed to occur stepwise by a successive release of segments of the background computational grids at a prescribed load. When a crack propagates it results in the release of segments between elements and is accompanied by a node doubling of the critical node when the magnitude of the configurational force is over a threshold value. Full details of the segment release for crack propagation modelling can be found in Miehe and Gurses [46], in which a similar algorithm is implemented in a FEM framework. The general step of the algorithm for crack propagation is visualized for a simple background mesh in Fig. 3.

However, there are some differences between FEM and MPM in solving problems involving crack propagation. As shown in Fig. 3(c), after alignment of the critical segment in direction of the configurational force, the shape of triangles that are attached to the critical segment will change accordingly. In conventional FEM, associated with this kind of element shape change, the integration points within these elements will also move to their relative positions. However, this is not the case in MPM, as shown in Fig. 3(c) and (d), the MPs within the triangles which have the critical segments are not moving during this process. It is the key point that distinguishes the current approach in the MPM framework from the method proposed by Miehe and Gurse [46]. Actually, it is also believed that this is the advantage of MPM in solving crack propagation problems through segment release and node doubling, especially for the elastoplastic materials in which several history-dependent variables are carried at integration points. If integration points move during the calculation process as they do in FEM, history-dependent variables need to be remapped to the new integration point positions, which will affect the final simulation results. However, this problem is prevented by the MPM framework, making the proposed method ideal for modelling elastoplastic problems.

However, it should be noted that the CF is implemented into the MPM framework for crack propagation modelling in linear elastic solids only in the present study. The crack propagation for elastoplastic problems requires additional computational procedures, which are beyond the scope current study and therefore is left for a future publication.

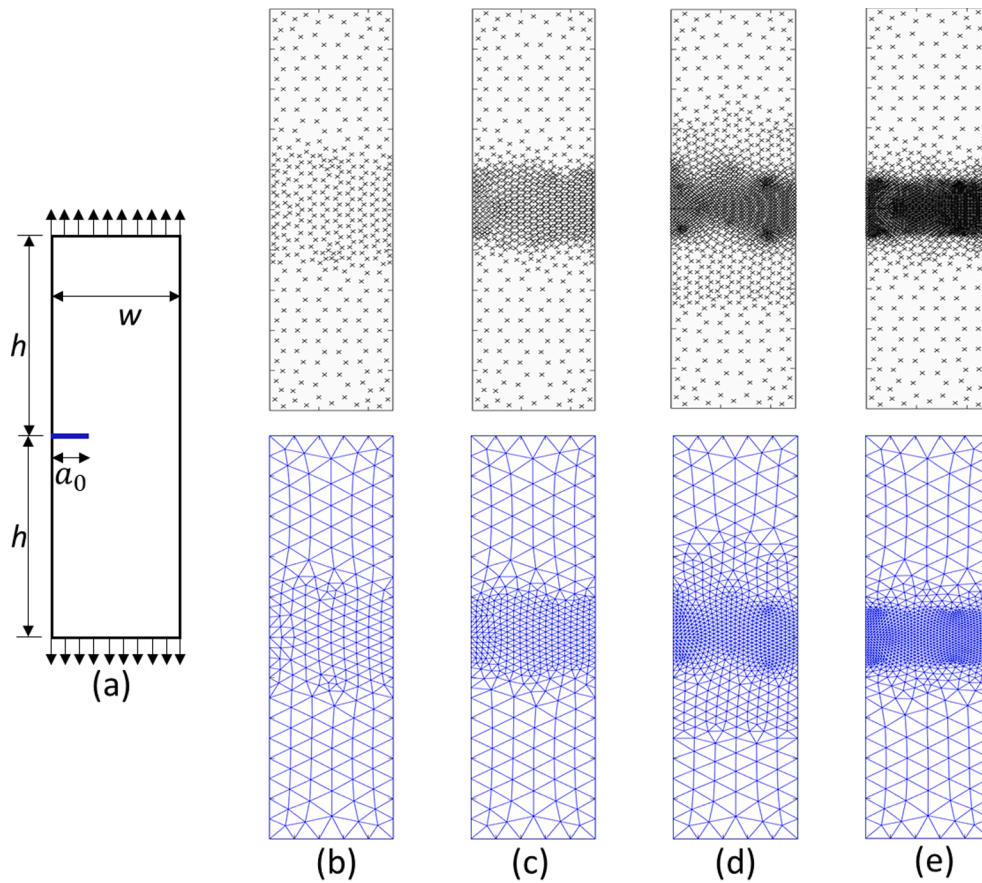


Fig. 4. Tensile test of single edge stationary crack problem. (a) Geometry and loading and different discretizations with (b) 384, (c) 790, (d) 1530 and (e) 2584 material points with 3-node background mesh.

4.2. Computational framework

In this paper, an implicit quasi-static formulation of MPM provides the computational platform for the deformation simulation, while the *CF* calculation and the crack propagation modelling are implemented through a post-processing procedure after obtaining convergence results for each load increment step. The configurational force vector is calculated on a stationary crack and then implemented as the fracture criteria for the crack propagation in linear elastic solids. The complete procedure of the computational framework is summarised as follows:

1. At the very beginning, the numerical MPM problem needs to be set up, which includes background computational grid generation, initial material points distribution and initial material point volume V_p^0 , etc. And then the applied external forces or displacements are split into a number of load steps, and for each of these steps, the following steps are undertaken;
2. For each MP, find influence elements of MP in the background mesh and evaluation of basis functions S_{vp} and their spatial derivatives ∇S_{vp} for all the nodes v of the influence elements;
3. Calculate the stiffness contribution, $[k^p]$, of all the MPs and assemble the individual contribution of each material point into the global stiffness matrix, $[K]$, through Eq. (10);
4. Calculate the internal force contribution, $\{f^{int}\}$, of all the MPs and assemble the contributions into the global force vector through Eq. (6);
5. Increment the external traction and/or body force in Eq. (6) and solve for the nodal displacements within a load step using the N-R process (see Eq. (13)) until the out-of-balance force reaching a specified convergence value (repeating steps 3 and 4 and updating

the spatial derivatives from step 2 to determine the current stiffness and internal force).

6. Update the material point positions, volume through interpolation from the incremental nodal displacements (See Eqs. (7) and (14));
7. Calculate the configurational force vector *CF* for the domain surrounding the crack tip through Eq. (27). The configurational force is calculated as a post-processing procedure after obtaining the stress and displacement field for MPs.
8. Check whether the crack criterion is violated. If it is, then releases the crack segment by doubling the critical nodes and update the background computational grids following the procedure described in Section 4.1.
9. Reset the background grid.

5. Numerical examples

In this section, several numerical examples are presented to demonstrate MPM combining the configurational force theory in solving fracture mechanics problems. The analysed problems cover tension, shear and three-point bending with single and multiple cracks. Some examples with complex crack patterns are also tested to show the performance of the proposed methodology.

5.1. Single edge stationary crack test

In order to estimate the accuracy of the material point method in predicting the configurational force vectors, we first consider the stationary crack problem in a single edge body with a simple linear elastic material behaviour under model-I loading. The benchmark is taken from the work of Miehe et al. [45]. The geometry of the problem is shown in

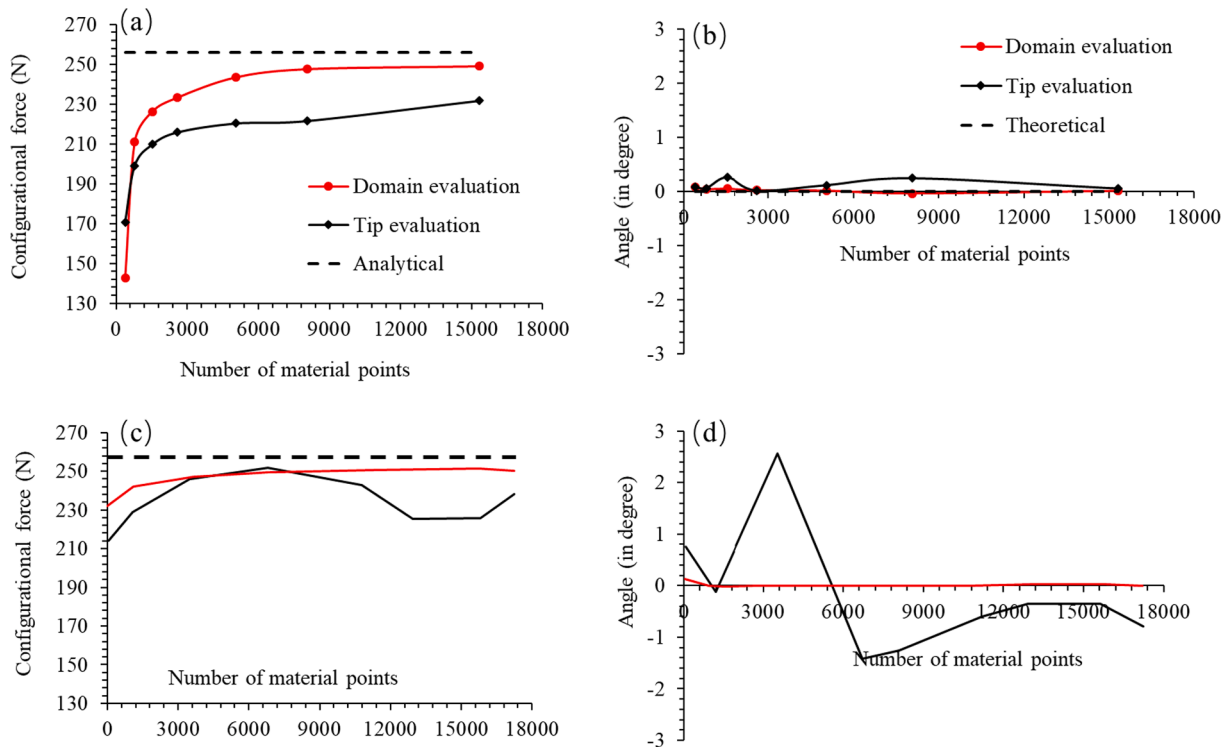


Fig. 5. Effect of discretization on both domain evaluation and crack-tip evaluation: (a) magnitude of configurational force; (b) potential crack propagation angle.

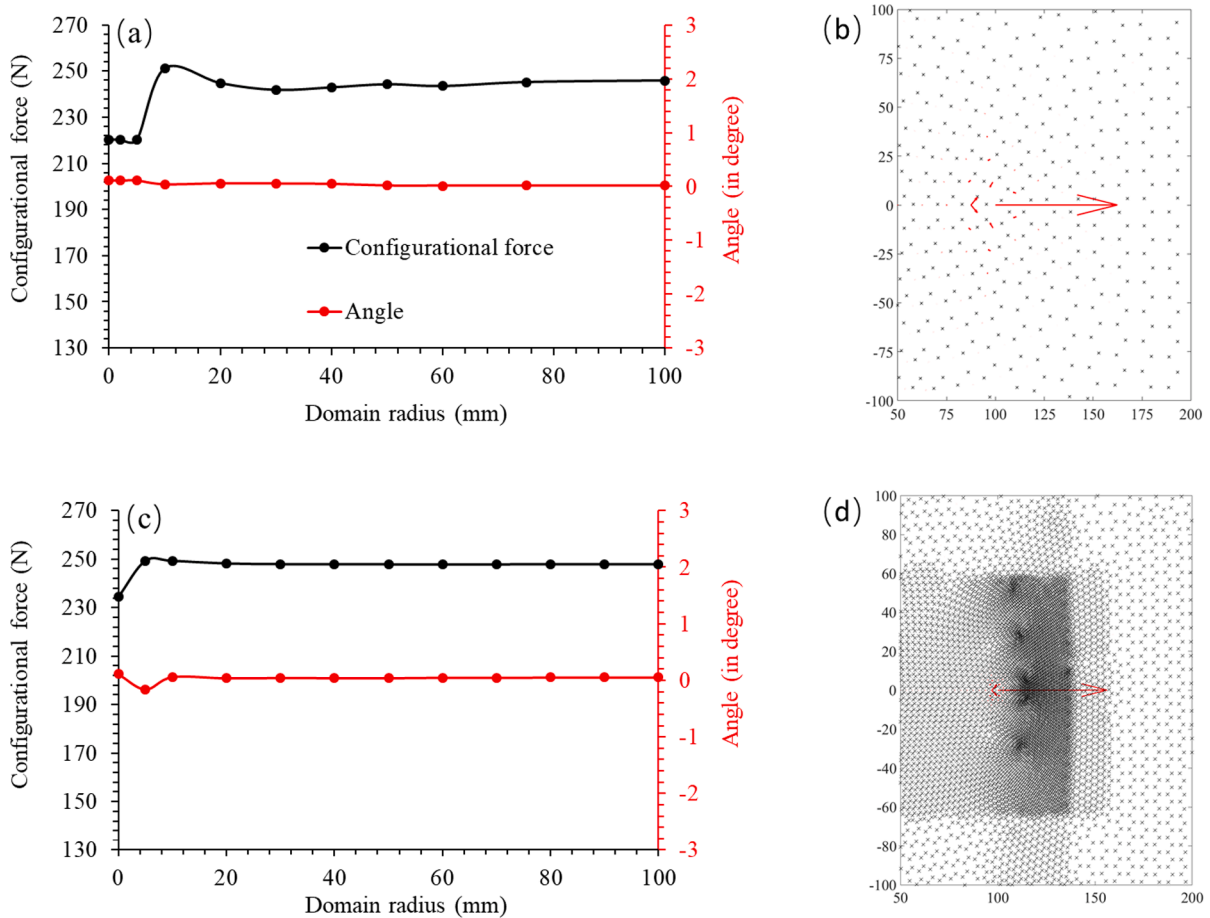


Fig. 6. Effect of the domain evaluation: (a) norm of configurational force and crack propagation angle for the discretization with 25; (b) configurational force distribution;

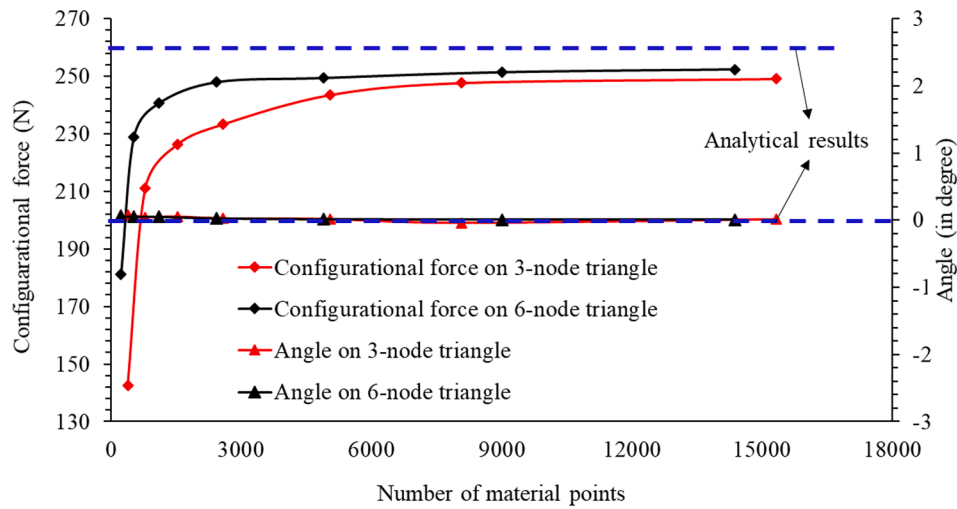


Fig. 7. Effect of type of computational grid on both norm of configurational force vector and crack propagation angle.

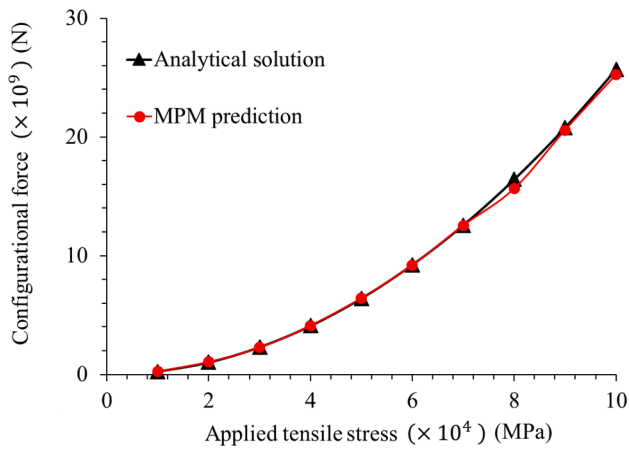


Fig. 8. Configurational forces under large deformation and comparisons with analytical solution [62].

Fig. 4, with height $h = 1000$ mm, width $w = 500$ mm and crack length $a_0 = 100$ mm. Furthermore, a linear elastic material model is used by defining two parameters Young's modulus $E = 210$ GPa and Poisson's ratio $\nu = 0.3$. A plane strain condition is assumed in the out-of-plane direction. For this stationary crack problem, traction with a tensile stress of 10 MPa is applied on top and bottom surfaces (shown in Fig. 4 (a)).

Similar to the work in Miehe et al. [45], we first extracted the

configurational force vector-only at the crack tip. Seven different discretizations, namely 384, 790, 1530, 2584, 5042, 8068 and 15,320 material points, are used for the solution of the physical problem and calculation of the configurational force vector. Fig. 4(b) through (e) show the first four of the material point distributions and their corresponding background mesh. The results for the norm of the configurational force vector and the potential crack propagation angles with the different discretizations are shown in Fig. 5(a) and (b), respectively. As shown, the results from the crack tip cannot provide uniform convergence values for both the norm of the configurational force vector and the propagation angle (due to the mode I nature of the problem the crack should propagate horizontally – a propagation angle of zero). Instead, the results are oscillating between the subsequent discretizations. Thus, an improvement method proposed by Denzer et al. [61] is also implemented in the present study. The key improvement of this method is that it calculates a resultant configurational force vector of an influence domain surrounding the crack tip instead of the configurational force at the crack tip. To this end, a domain with radius $R = 50$ mm around the crack tip was defined (the impact of the radius size is discussed later in this section). The corresponding results in terms of the norm of configurational force and the crack propagation angle are also presented for comparison in Fig. 5 (a) and (b) respectively. Clearly, results obtained from this domain evaluation yield a better convergence behaviour than those obtained from the above only crack-tip evaluation. However, there is still a discrepancy between analytical and computational results. And this discrepancy can be traced back to the background grid being discretised with constant strain triangles. Improvement may be sought via a higher-order triangle element (e.g. linear strain triangle element, such as 6-node triangles), which will be discussed later. The results from the

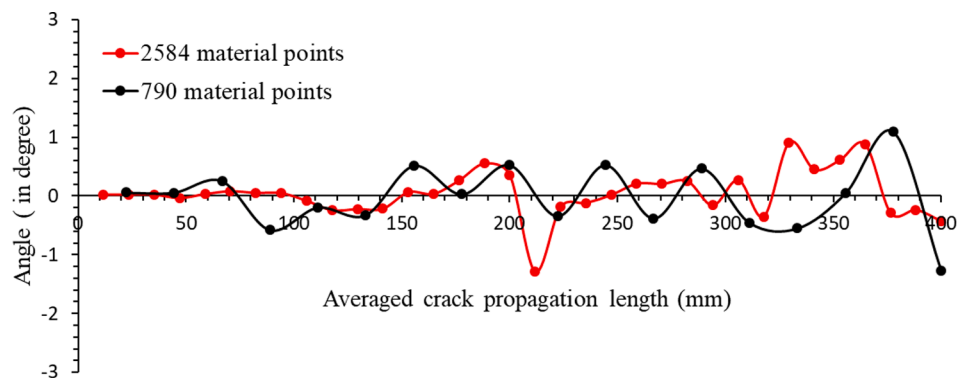


Fig. 9. Crack propagation in single edge crack sample.

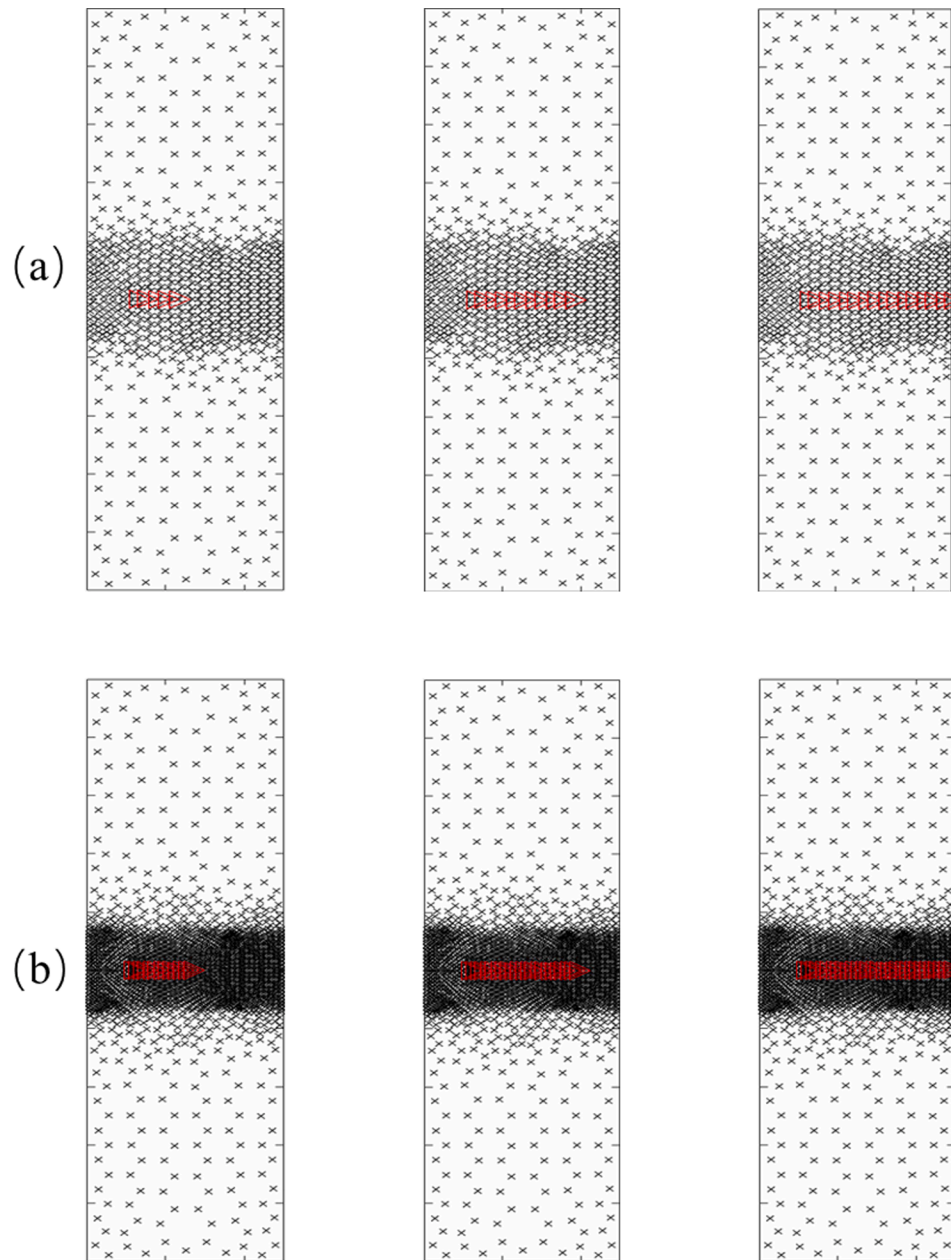


Fig. 10. Crack propagation trajectories during the loading process for two different discretizations (the red arrows show the crack propagation path): (a) 790 material point; (b) 2584 material points. (For interpretation of the references to colour in this figure legend, the reader is referred to the web version of this article.)

present simulation are also compared with the FEM in [45] where constant strain triangles are used for the discretization. Fig. 5(c) and (d) show the corresponding FEM results in terms of the norm of configurational force and the crack propagation angle, respectively. It can be clearly observed that the FEM can generally obtain better results for the norm of configurational force with coarse grids; however, when the grids are refined, two methods predict similar results which are very close to the analytical solution, especially for the domain evaluation. Regarding the crack propagation angle, the MPM can generally obtain a quicker convergence than the FEM, especially for the tip evaluation. From the comparison, it is reasonable to believe that the accuracy of the present simulation is acceptable and can be used for further crack propagation problems.

In order to obtain a convergence result regarding the size of the selected domain radius. Several different radii of the domain are defined to investigate the effect of the domain size on the evaluation of the resultant configurational force vector based on the background mesh

with 2584 elements and material points. The results for the norm of the configurational force vector and the potential crack propagation angles are depicted in Fig. 6(a). As shown, the results show an almost constant value/direction of the configurational force regardless of the domain size after a critical domain radius (around 50 mm in terms of the angle of propagation). Thus, a domain with a radius $R = 50$ mm surrounding the crack tip is considered for this case. This size is equivalent to one-twentieth of the length of the original crack. Therefore, the domain size is set as around one-twentieth of the length of the initial crack in the remainder of this paper. It has been demonstrated that there is a relationship between the configurational force and the traditional J-integral in fracture mechanics [24,41,42]. The J-integral can be regarded as the projection of the configurational force to the crack extension. Therefore, the configurational force obtained should be path-dependent for a linear elastic material model. However, the accuracy of the numerical evaluation of the configurational force strongly depends on the accuracy of the Eshelby stress in the vicinity of the crack tip. Owing to the singular

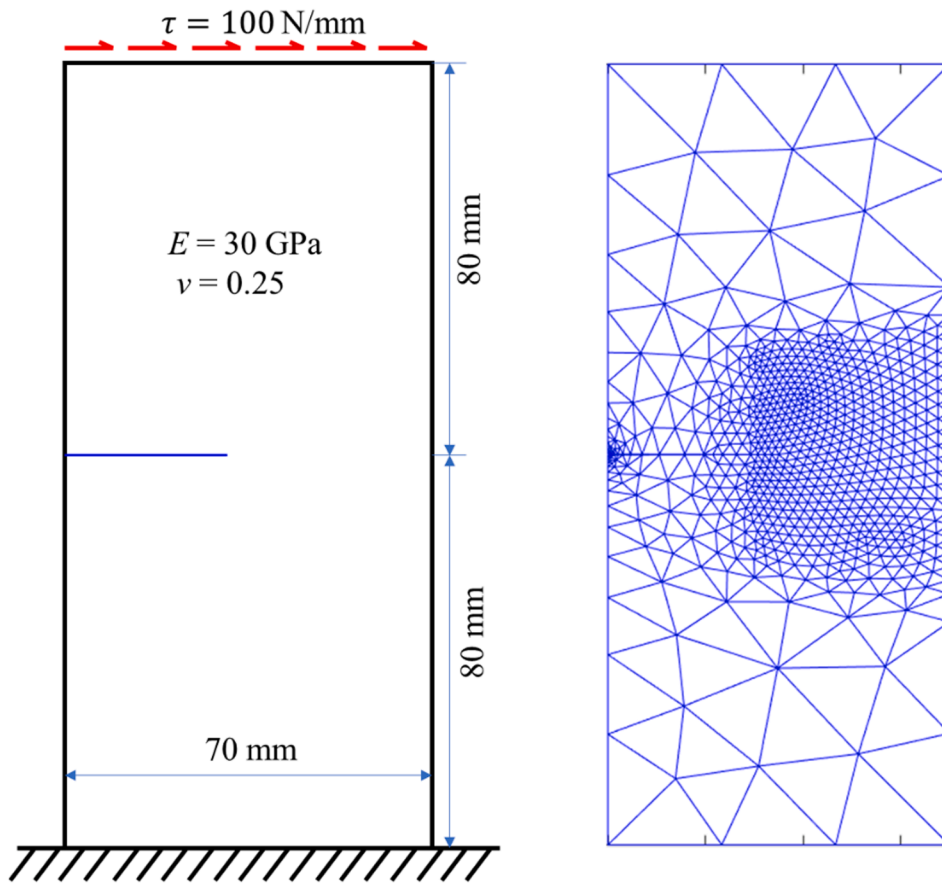


Fig. 11. Single edge crack under shear test and the corresponding background mesh.

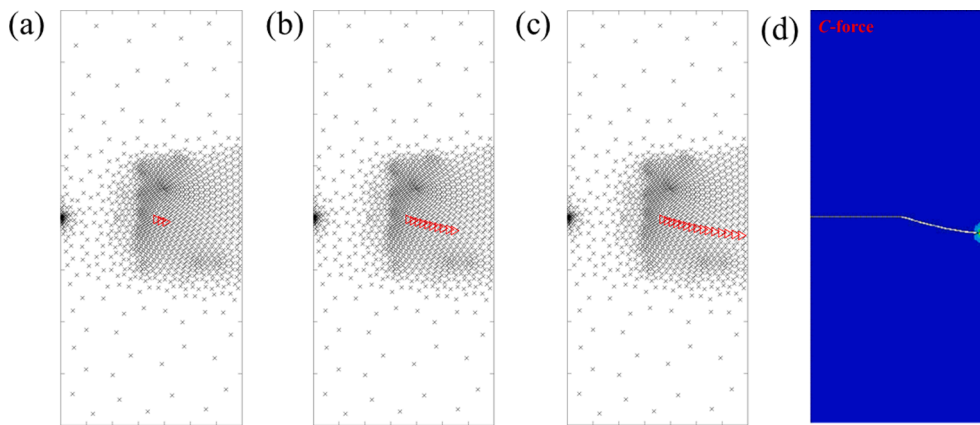


Fig. 12. Crack propagation trajectory of single edge cracked plate under shear test: (a) propagation steps = 3; (b) propagation steps = 10; (c) propagation steps = 15; (d) final crack pattern from FEM prediction [40].

behavior of the spatial motion stresses and strain near the crack tip, the accuracy of Eshelby stress is often insufficient within a finite element setting. For an improvement, a domain evaluation is needed to get a convergence value for the Eshelby stress. Therefore, the physical meaning of the critical domain radius is actually the critical domain beyond which the numerically obtained configurational force is size-independent (J-integral path-independent).

Fig. 6(b) presents the distribution of the configurational force within the specimen. It is observed that the configurational force vectors appear mostly at the crack-tip node and almost vanish with a distance less than 20 mm from the crack tip. It further confirms that the resultant configurational vector can achieve a convergence when a reasonable

domain is chosen (radius $R > 20$ mm). It should be pointed out here that the directions of configurational forces are depicted coincide with the direction of crack propagation in the present study, which may be different from other published literature [41,43]. The direction shown in this way can give a direct impression that the configurational force can be considered as the crack driving force.

It should be mentioned here that a convergent domain size depends on the mesh size. As it is shown in Fig. 6, a finer discretization can generally reach convergence with a smaller domain size. By specifically, the norm of configurational force and the potential crack propagation angle are convergent beyond a domain radius of 20 mm for the discretization with 2584 material points while they can get convergence

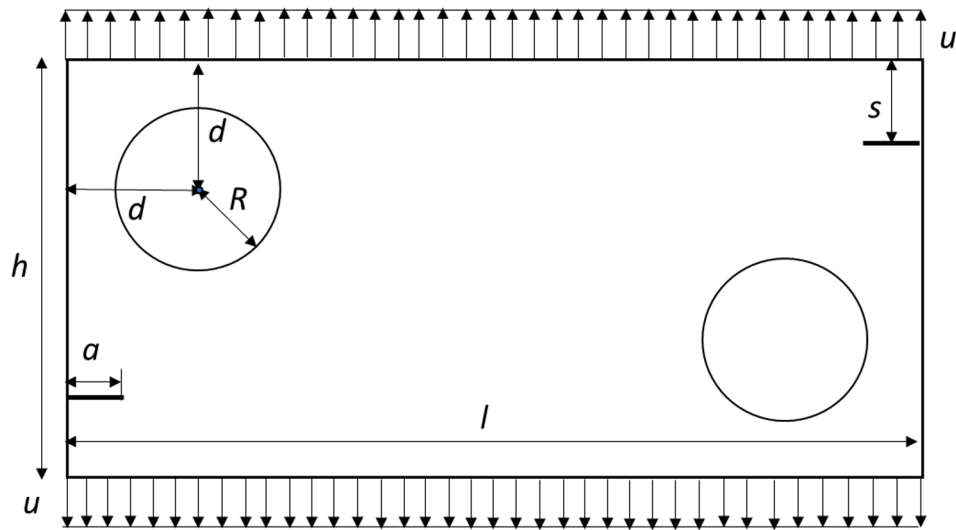


Fig. 13. Geometry and loading of tensile test.

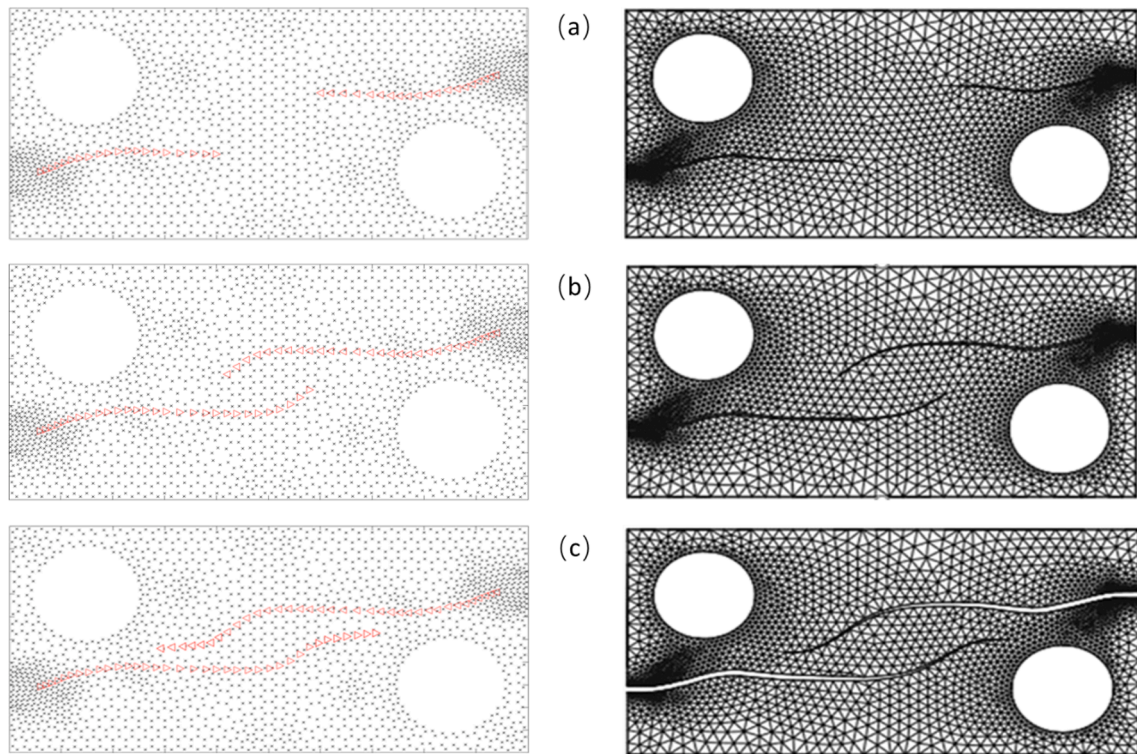


Fig. 14. Crack propagation trajectories comparison: material point method from the current study (left) and finite element method (right) from [45].

with a domain radius around 10 mm for the discretization with 8068 material points. According to the FEM results in [45], for the mesh with 7258 elements, results including the configurational force and the potential angle reach convergence with a domain radius around 15 mm. In addition, it can be observed from the distribution of the configurational force in Fig. 6(b) and (d) that the configurational force vectors appear mostly within 3 to 4 layers of elements around the crack tip and vanish outside this domain, which is consistent with the FEM results in [61]. Therefore, it is reasonable to conclude that the MPM can present similar results with FEM regarding the size of the selected domain radius.

As stated in Section 2.3, two kinds of triangular elements, namely the constant strain triangle element and the linear strain triangle element are mostly used in the mesh-based numerical simulations. It is generally

recognised that the 3-node triangle element may give low accurate results due to its low order basis functions. To this end, the 6-node triangle is also included in the present study for comparison. As shown in Fig. 2, the number of material points has increased by three times with such a computational grid. The results in terms of the configurational force vectors, including the magnitude and potential propagation angle, of these two kinds of elements, are shown in Fig. 7. As shown, the 3-node triangle element can generally give similar results with 6-node triangles for both the magnitude of the configurational force and the propagation angle, although more accurate results may be achieved by 6-node triangles. Both results become very close to the analytical values (256 N for configurational force and 0° for propagation angle) when the discretization is fine enough. In consideration of the computational cost

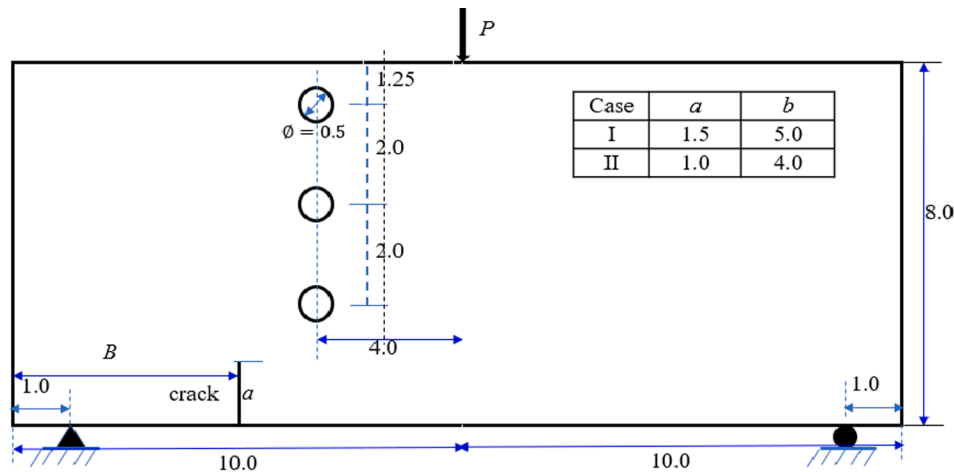


Fig. 15. Cracked beam with three holes under three-point bending (all dimensions in mm).

and additional effort in the 6-node triangle element in achieving crack propagation by releasing segments, the computational results with the 3-node triangle grid can be considered to be acceptable. This is further underlined by the subsequent examples which demonstrate the predictive capabilities of the formulation to capture experimentally observed curved crack trajectories. Therefore, the 3-node triangle computational grid will be adopted, hereafter.

It should be emphasized here that the most attractive point of MPM in commercial application in recent years is its application in large deformation. To show the performance of the current framework in large deformation, the approach proposed in the present study is also used to simulate the stationary single edge crack under large tensile deformation. Large tensile stresses vary from 10^4 to 10^5 MPa are applied on the top boundary of the specimen which would produce large tensile engineering strains around 5–50%. The norm of the configurational force is calculated accordingly for each case. Fig. 8 shows the comparisons of numerical predictions from the present framework and the analytical solution in [62]. As it can be clearly observed, the MPM predictions agree very well with the analytical solutions even under large deformations up to 50% strain. Beyond this value, the standard MPM framework may suffer a nonphysical numerical fracture problem from our preliminary simulations. CPDI MPM approaches [33,63] may be used to solve this numerical fracture problem, but it is beyond of the scope of current research. On the other hand, the numerical example with the same background mesh is also modelled with a commercial FEM software ANSYS [64]. From our preliminary simulations, the maximum strain can be simulated with ANSYS is up to around 32% beyond which it would stop with errors due to serious distortion of elements near the crack tip. Therefore, it is reasonable to believe the approach proposed in the present study is ready for large deformation crack modelling and has certain advantages over conventional FEM. In addition, it should be also noted that the strain to failure for typical engineering materials is much less than that which will produce numerical fracture. Therefore, it is more necessary to employ a softening and/or damage model that degrades the strength and/or stiffness of the material so that the deformation beyond the physical failure strain is well predicted. And this will be incorporated into the MPM framework for modelling the fracture behaviour of elastoplastic materials, which will be reported in a future publication.

5.2. Crack propagation under tension

In this section, the crack propagation for the single edge notched specimen is simulated. To this end, the same specimen as described in Section 5.1 but with a displacement control on the upper and bottom boundary is considered. The computation of the configurational force is

based on the domain evaluation with $R = 50$ mm in discretization with 2584 material points in a 3-node triangle background mesh. The critical release energy release rate (i.e. the criteria for crack propagation) is set to be $g_c = 1$ N/mm. The rest of the material properties are the same as in Section 5.1.

Fig. 9 shows the crack propagation angle over the full crack length for two discretizations, namely 790 material points and 2584 material points, respectively. As it can be observed, the predicted propagation angles show no uniform convergence behaviour and are oscillating for these two discretizations. Generally, fine discretization can give more accurate results. As shown, the angles determined from 790 material points oscillate around the expected value of 0° in a range between -1.5° and 1.5° . For the discretization with 2580 material points, the oscillation is observed to reduce between -1.2° and 1° , see Fig. 9. However, concerning an average of the crack propagation angles, the results from both two discretizations are very close to the expected value of 0° . This is further demonstrated in Fig. 9, where the crack propagation path is shown for these two discretizations. The crack almost propagates along the centre line during all the loading process, nearly no deviation can be observed for two discretizations. This demonstrates the successful implementation of the configurational force fracture criteria in the MPM framework for predicting the crack propagation in linear elastic solids. It should be noted that each crack propagation step in Fig. 10 is associated with a critical segment release at the crack tip as described in Section 4.1.

5.3. Crack propagation under shear

This case corresponds to the crack propagation of an edge crack in a plate under shear loading. The geometrical dimensions are shown in Fig. 11, where the width, height and the initial crack length of the plate are 70, 160 and 35 mm respectively. The plate is fixed at the bottom while shear stress, $\tau = 100$ N/mm, is applied along the top edge. The material properties of the plate are $E = 206.8$ GPa and $\nu = 0.25$. The plate is discretized with 1418 material points as shown in Fig. 12, much more intensive material points distribution is around the crack tip. The problem is solved in 15 steps. The crack propagation trajectory in 3, 10 and 15 steps are shown in Fig. 12(a) to (c) while the final crack pattern from FEM in [40] is shown in Fig. 12(d). As shown, the predicted crack propagates downward at the beginning and then tends to parallel to the horizontal line gradually which agrees well with the results from FEM [40]

5.4. Crack propagation with holes

In this part, a problem containing two propagating cracks is studied.

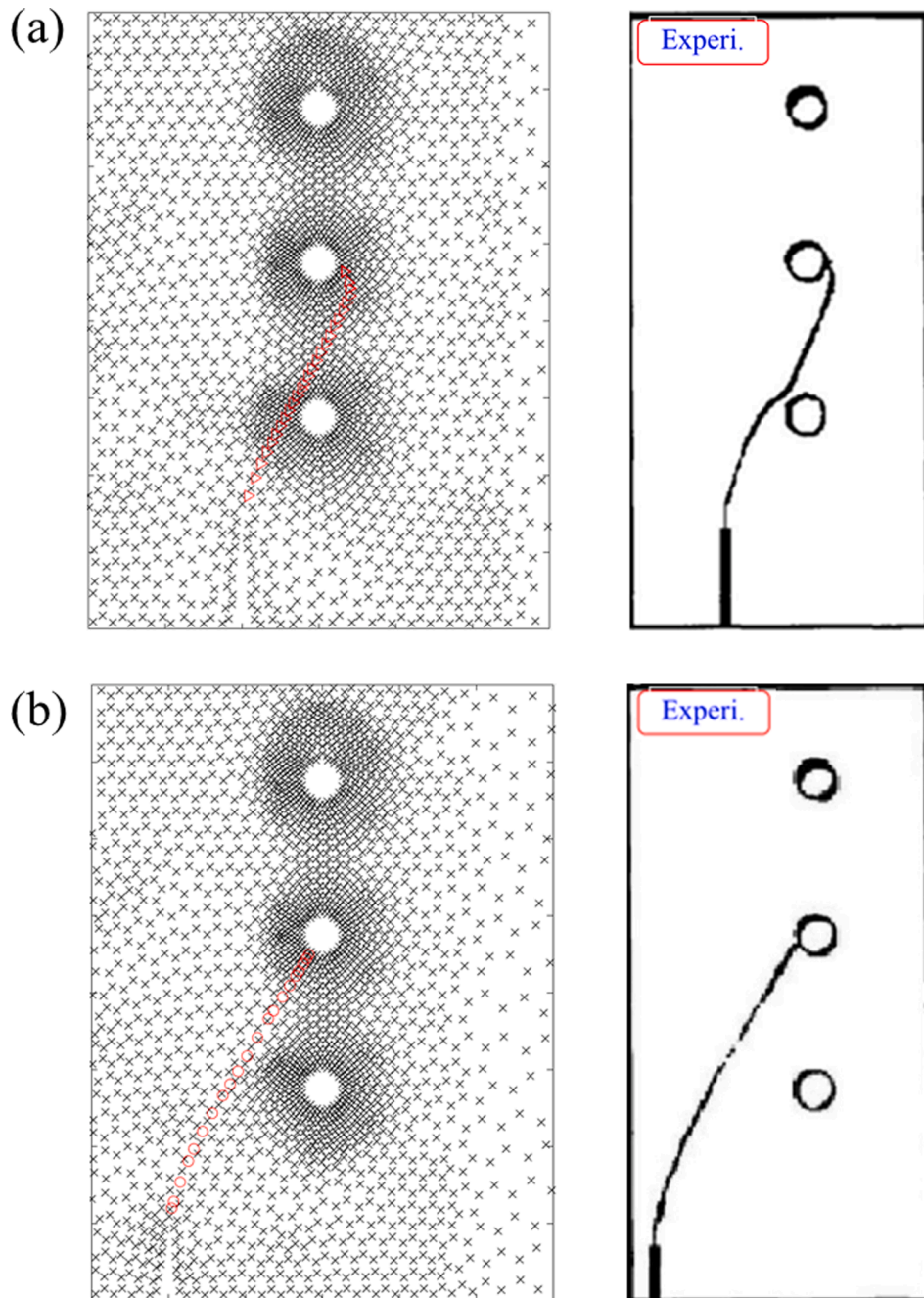


Fig. 16. Comparison of the final crack paths between numerical predictions and experimental results [66]: (a) case I; (b) case II.

The benchmark for this problem is taken from Bouchard et al. [65], in which a pre-cracked body with two holes and two cracks under tensile test was studied. The detailed geometrical dimension of this model is $l = 20$, $h = 10$, $a = 1$, $h_0 = 2.85$, $R = 2$ and $d = 3$ mm, as shown in Fig. 13. The material with the elasticity modulus $E = 20.8$ GPa, Poisson's ratio $\nu = 0.3$ and the critical energy release rate $g_c = 1$ N/mm is adopted here. Displacement loadings were applied on the top and bottom boundaries with $u = 2$ mm.

Different from the single crack propagation problem discussed above, we need to consider the two crack propagations separately in this example. Therefore, after each loading step, one has to compute independently the configurational force vector of each crack tip. And then the crack propagations at the two crack tips are treated one after the other, according to their corresponding configurational force vectors.

The resulting crack propagation trajectories are shown in Fig. 14.

Both cracks first show a tendency to propagate towards the hole and then reorient themselves horizontally once they passed the holes. These simulations are in good agreement with the results reported in [45,65], where the traditional finite element method was used, and demonstrate the method's ability to simulate multiple propagating cracks.

It is also interesting to find that although the phase-field approach is considered to be a powerful tool in solving crack propagation problems, it fails to obtain satisfied crack paths with holes according to Wu et al. [23]. However, this is not the case in the present study, which further demonstrates the great advantages of the combined MPM and CF approach in predicting the crack propagation path.

5.5. Crack propagation under three-point bending

This example corresponds to a cracked beam with three holes under

three-point bending. The geometrical dimensions and initial boundary conditions are illustrated in Fig. 15. Two test cases, I and II, which have different initial crack lengths and crack offset values (as shown a and b in Fig. 15) have been considered. Both beams are loaded through a concentrated force, $P = 50$ N at the middle of the top edge. The experimental tests for these two examples with polymethylmethacrylate can be found in [66] and numerical tests are also available in published literature (e.g. [23,40,67]).

In the present simulations, the material properties, $E = 3.3$ GPa and $\nu = 0.35$ are taken from [66]. Similar discretizations (around 3500 material points) are used for the two different cases.

The final numerical predicted crack patterns for the two different cases are compared with experimental results in Fig. 16. It can be observed that the numerical predicted crack propagation paths are consistent with experimental observations in both cases. By specifically, in case I, where the initial crack and holes are not close enough, the crack passes towards the bottom hole and deflects to the opposite side when it is close to the bottom hole and finally arrives at the right hand of the middle hole; while in the case II, where the initial crack is close to the holes, the crack propagation path is attracted by the bottom hole and eventually arrested by it. The above phenomenon is well captured by the proposed model, which demonstrates its ability in predicting fracture propagation interacting with holes.

6. Conclusions

This paper has presented the development of a new platform to coupling the material force and MPM for crack modelling in 2D and takes advantage of both the material force approach and the MPM. Basically, an implicit quasi-static formulation of the MPM provides the computational platform for the deformation simulation, while the CF calculation and the crack propagation modelling are implemented through a post-processing procedure after obtaining convergence results for stress and displacement field at each load increment step.

In terms of the numerical results, the CF vector was first calculated on a stationary crack problem. Evaluations at the crack-tip node and within domains were presented. Results show that the domain approach can generally provide better accuracy than the crack-tip node only method. After comparing the results from two background computational grids, i.e. 3-node and 6-node triangles, 3-node triangle background computational grid is chosen for the present study considering the computational cost the complexity that the 6-node triangle may bring in crack propagations. The domain-based configurational force vector evaluation was then implemented in the MPM framework as the fracture criteria for the crack propagation in linear elastic solids. Crack propagation was achieved by segment release and node doubling in the background grids. Several examples, including the single edge cracked plate under tension, shear and multiple cracks as well as a cracked beam with three holes under three-point bending, were simulated with the proposed combined model. All simulated results in terms of the crack propagation path resemble favourably the corresponding observations from the literature, which demonstrates the abilities of the proposed model in predicting the crack propagation in linear-elastic solids.

At present, the numerical platform has been realised in the 2D model. In principle, the algorithm can be easily extended to 3D, and by doing so the full advantages of material force criterion and the material point method in solving crack propagation problems over finite element method can be accommodated in a unified framework. Of course, such a complete 3D model will pose much-increased demand in terms of computational cost, and in this respect enhancement in the computational efficiency will require dedicated research. In addition, the crack propagation problems for elastic-plastic materials, which require additional efforts in dealing with dynamic varying fracture criteria, are not presented in the current paper. This topic is considered to be significant enough to be the focus of a future study and will be reported in a separate paper.

CRediT authorship contribution statement

Rongxin Zhou: Conceptualization, Data curation, Formal analysis, Investigation, Methodology, Resources, Software, Validation, Visualization, Writing – original draft, Writing – review & editing. **William M. Coombs:** Conceptualization, Funding acquisition, Methodology, Project administration, Resources, Software, Supervision, Validation, Visualization, Writing – review & editing. **Yang Xu:** Conceptualization, Methodology, Software, Validation, Visualization, Writing – original draft, Writing – review & editing. **Ping Zhang:** Methodology, Software, Validation, Visualization, Writing – review & editing. **Li-Ge Wang:** Methodology, Software, Validation, Visualization, Writing – review & editing.

Declaration of Competing Interest

The authors declare that they have no known competing financial interests or personal relationships that could have appeared to influence the work reported in this paper.

Acknowledgement

This work was supported by the Engineering and Physical Sciences Research Council [grant numbers EP/M017494/1]. All data created during this research are openly available at collections.durham.ac.uk/ (specific doi to be confirmed if/when the paper is accepted).

References

- [1] E. Gürses, C. Miehe, A computational framework of three-dimensional configurational-force-driven brittle crack propagation, *Comput. Methods Appl. Mech. Eng.* 198 (15-16) (2009) 1413–1428, <https://doi.org/10.1016/j.cma.2008.12.028>.
- [2] A. Jenabidehkordi, Computational methods for fracture in rock: a review and recent advances, *Front Struct. Civ. Eng.* 13 (2) (2019) 273–287, <https://doi.org/10.1007/s11709-018-0459-5>.
- [3] T. Rabczuk, Computational methods for fracture in brittle and quasi-brittle solids: state-of-the-art review and future perspectives, *ISRN Appl Math* 2013 (2013) 1–38, <https://doi.org/10.1155/2013/849231>.
- [4] R. Zhou, Z. Song, Y. Lu, 3D mesoscale finite element modelling of concrete, *Comput. Struct.* 192 (2017) 96–113.
- [5] R. Zhou, H.-M. Chen, Mesoscopic investigation of size effect in notched concrete beams: the role of fracture process zone, *Eng. Fract. Mech.* 212 (2019) 136–152, <https://doi.org/10.1016/J.ENGFRACMECH.2019.03.028>.
- [6] R.d. Borst, J.J.C. Remmers, A. Needleman, M.-A. Abellan, Discrete vs smeared crack models for concrete fracture: Bridging the gap, *Int. J. Numer. Anal. Meth. Geomech.* 28 (78) (2004) 583–607, [https://doi.org/10.1002/\(ISSN\)1096-985310.1002/nag.v28:7/810.1002/nag.374](https://doi.org/10.1002/(ISSN)1096-985310.1002/nag.v28:7/810.1002/nag.374).
- [7] M. Cervera, M. Chiumenti, R. Codina, Mixed stabilized finite element methods in nonlinear solid mechanics. Part II: Strain localization, *Comput. Methods Appl. Mech. Eng.* 199 (37-40) (2010) 2571–2589, <https://doi.org/10.1016/j.cma.2010.04.005>.
- [8] M. Cervera, M. Chiumenti, Mesh objective tensile cracking via a local continuum damage model and a crack tracking technique, *Comput. Methods Appl. Mech. Eng.* 196 (1-3) (2006) 304–320, <https://doi.org/10.1016/j.cma.2006.04.008>.
- [9] S. Kruch, Nonlocal damage theory, *Am. Soc. Mech. Eng. Appl. Mech. Div. AMD 142* (1992) 83–96. Publ by ASME.
- [10] Z.P. Bažant, G. Pijaudier-Cabot, Nonlocal continuum damage, localization instability and convergence, *J. Appl. Mech. Trans. ASME* 55 (1988) 287–293, <https://doi.org/10.1115/1.3173674>.
- [11] E. Martínez Pañeda, *Strain Gradient Plasticity-Based Modeling of Damage and Fracture*, Springer International Publishing, Cham, 2018. <https://doi.org/10.1007/978-3-319-63384-8>.
- [12] E. Barchiesi, H. Yang, C.A. Tran, L. Placidi, W.H. Müller, Computation of brittle fracture propagation in strain gradient materials by the FEniCS library, *Math. Mech. Solids* 26 (3) (2021) 325–340, <https://doi.org/10.1177/1081286520954513>.
- [13] J. Li, A strain gradient model for fracture prediction in brittle materials, *J. Appl. Mech. Trans. ASME* 75 (2008) 0210041–210049, <https://doi.org/10.1115/1.2775498>.
- [14] P.A. Cundall, O.D.L. Strack, A discrete numerical model for granular assemblies, *Géotechnique* 29 (1) (1979) 47–65, <https://doi.org/10.1680/geot.1979.29.1.47>.
- [15] Y. Lu, Modelling the dynamic response of concrete with mesoscopic heterogeneity, in: J. Weerheijm (Ed.), *Underst. Tensile Prop. Concr.*, Woodhead Publishing Series in Civil and Structural Engrg., 2013, pp. 218–67. <https://doi.org/10.1533/9780857097538.2.218>.

- [16] G.T. Camacho, M. Ortiz, Computational modelling of impact damage in brittle materials, *Int. J. Solids Struct.* 33 (20-22) (1996) 2899–2938, [https://doi.org/10.1016/0020-7683\(95\)00255-3](https://doi.org/10.1016/0020-7683(95)00255-3).
- [17] R. Zhou, Y. Lu, A mesoscale interface approach to modelling fractures in concrete for material investigation, *Constr. Build. Mater.* 165 (2018) 608–620.
- [18] R. Zhou, H.-M. Chen, Y. Lu, Mesoscale modelling of concrete under high strain rate tension with a rate-dependent cohesive interface approach, *Int. J. Impact Eng.* 139 (2020) 103500, <https://doi.org/10.1016/j.ijimpeng.2020.103500>.
- [19] N. Sukumar, N. Moës, B. Moran, T. Belytschko, Extended $\bar{\nu}$ Element Method for Three-dimensional Crack Modelling, vol. 48, 2000.
- [20] T.-P. Fries, T. Belytschko, The extended/generalized finite element method: an overview of the method and its applications, *Int. J. Numer. Meth. Eng.* 84 (3) (2010) 253–304, <https://doi.org/10.1002/nme.v84:310.1002/nme.2914>.
- [21] M. Jirásek, Comparative study on finite elements with embedded discontinuities, *Comput. Methods Appl. Mech. Eng.* 188 (1-3) (2000) 307–330, [https://doi.org/10.1016/S0045-7825\(99\)00154-1](https://doi.org/10.1016/S0045-7825(99)00154-1).
- [22] A. Staroselsky, R. Acharya, B. Cassenti, Phase field modeling of fracture and crack growth, *Eng. Fract. Mech.* 205 (2019) 268–284, <https://doi.org/10.1016/j.engfracmech.2018.11.007>.
- [23] J.Y. Wu, V.P. Nguyen, C.T. Nguyen, D. Sutula, S. Sinaie, S.P.A. Bordas, Phase-field modeling of fracture, *Adv. Appl. Mech.* 53 (2020) 1–183, <https://doi.org/10.1016/bs.aams.2019.08.001>.
- [24] W. Ai, R.E. Bird, W.M. Coombs, C.E. Augarde, A configurational force driven cracking particle method for modelling crack propagation in 2D, *Eng Anal Bound Elem* 104 (2019) 197–208, <https://doi.org/10.1016/j.enganabound.2019.03.008>.
- [25] T. Rabczuk, G. Zi, S. Bordas, H. Nguyen-Xuan, A simple and robust three-dimensional cracking-particle method without enrichment, *Comput. Methods Appl. Mech. Eng.* 199 (37-40) (2010) 2437–2455, <https://doi.org/10.1016/j.cma.2010.03.031>.
- [26] T. Rabczuk, T. Belytschko, A three-dimensional large deformation meshfree method for arbitrary evolving cracks, *Comput. Methods Appl. Mech. Eng.* 196 (29-30) (2007) 2777–2799, <https://doi.org/10.1016/j.cma.2006.06.020>.
- [27] R.W. Macek, S.A. Silling, Peridynamics via finite element analysis, *Finite Elem. Anal. Des.* 43 (15) (2007) 1169–1178, <https://doi.org/10.1016/j.finel.2007.08.012>.
- [28] S. Liu, G. Fang, J. Liang, M. Fu, B. Wang, A new type of peridynamics: element-based peridynamics, *Comput. Methods Appl. Mech. Eng.* 366 (2020) 113098, <https://doi.org/10.1016/j.cma.2020.113098>.
- [29] X. Chen, M. Gunzburger, Continuous and discontinuous finite element methods for a peridynamics model of mechanics, *Comput. Methods Appl. Mech. Eng.* 200 (9-12) (2011) 1237–1250, <https://doi.org/10.1016/j.cma.2010.10.014>.
- [30] M.R. Tupek, J.J. Rimoli, R. Radovitzky, An approach for incorporating classical continuum damage models in state-based peridynamics, *Comput. Methods Appl. Mech. Eng.* 263 (2013) 20–26, <https://doi.org/10.1016/j.cma.2013.04.012>.
- [31] F. Mossaiby, A. Shojaei, M. Zaccariotto, U. Galvanetto, OpenCL implementation of a high performance 3D Peridynamic model on graphics accelerators, *Comput. Math Appl.* 74 (8) (2017) 1856–1870, <https://doi.org/10.1016/j.camwa.2017.06.045>.
- [32] D. Sulsky, Z. Chen, H.L. Schreyer, A particle method for history-dependent materials, *Comput. Methods Appl. Mech. Eng.* 118 (1-2) (1994) 179–196, [https://doi.org/10.1016/0045-7825\(94\)90112-0](https://doi.org/10.1016/0045-7825(94)90112-0).
- [33] V.P. Nguyen, C.T. Nguyen, T. Rabczuk, S. Natarajan, On a family of convected particle domain interpolations in the material point method, *Finite Elem. Anal. Des.* 126 (2017) 50–64, <https://doi.org/10.1016/j.finel.2016.11.007>.
- [34] A. Nair, S. Roy, Implicit time integration in the generalized interpolation material point method for finite deformation hyperelasticity, *Mech. Adv. Mater. Struct.* 19 (6) (2012) 465–473, <https://doi.org/10.1080/15376494.2010.550082>.
- [35] A. De Vaucorbeil, V.P. Nguyen, S. Sinaie, J.Y. Wu, Material point method after 25 years: theory, implementation, and applications, *Adv. Appl. Mech.* 53 (2020) 185–398, <https://doi.org/10.1016/bs.aams.2019.11.001>.
- [36] P. Yang, Y. Gan, X. Zhang, Z. Chen, W. Qi, P. Liu, et al., Improved decohesion modeling with the material point method for simulating crack evolution, *Int. J. Fract.* 186 (2014) 177–184, <https://doi.org/10.1007/s10704-013-9925-1>.
- [37] J. Wretborn, P.M. Supervisor, R. Armiento, Modelling cracks in solid materials using the Material Point Method, n.d.
- [38] Y.J. Guo, J.A. Nairn, Three-dimensional dynamic fracture analysis using the material point method, *C – Comput. Model Eng. Sci.* 16 (2006) 141–155, <https://doi.org/10.3970/cmcs.2006.016.141>.
- [39] R. Zhou, P. Zhu, Z. Li, The shielding effect of the plastic zone at mode-II crack tip, *Int. J. Fract.* 171 (2) (2011) 195–200, <https://doi.org/10.1007/s10704-011-9627-5>.
- [40] Y. Guo, Q. Li, Material configurational forces applied to mixed mode crack propagation, *Theor. Appl. Fract. Mech.* 89 (2017) 147–157, <https://doi.org/10.1016/j.tafmec.2017.02.006>.
- [41] K. Özenc, M. Kaliske, G. Lin, G. Bhashyam, Evaluation of energy contributions in elasto-plastic fracture: a review of the configurational force approach, *Eng. Fract. Mech.* 115 (2014) 137–153, <https://doi.org/10.1016/j.engfracmech.2013.11.001>.
- [42] N. Simha, F. Fischer, G. Shan, C. Chen, O. Kolednik, J-integral and crack driving force in elastic-plastic materials, *J. Mech. Phys. Solids* 56 (9) (2008) 2876–2895, <https://doi.org/10.1016/j.jmps.2008.04.003>.
- [43] O. Kolednik, R. Schöngrundner, F.D. Fischer, A new view on J-integrals in elastic-plastic materials, *Int. J. Fract.* 187 (1) (2014) 77–107, <https://doi.org/10.1007/s10704-013-9920-6>.
- [44] J.D.E. Shelby, The force on an elastic singularity, *Philos Trans R Soc London Ser A, Math Phys Sci* 244 (1951) 87–112, <https://doi.org/10.1098/rsta.1951.0016>.
- [45] C. Miehe, E. Gürses, M. Birkle, A computational framework of configurational-force-driven brittle fracture based on incremental energy minimization, *Int. J. Fract.* 145 (4) (2007) 245–259, <https://doi.org/10.1007/s10704-007-9078-1>.
- [46] C. Miehe, E. Gürses, A robust algorithm for configurational-force-driven brittle crack propagation with R-adaptive mesh alignment, *Int. J. Numer. Meth. Eng.* 72 (2) (2007) 127–155, [https://doi.org/10.1002/\(ISSN\)1097-020710.1002/nme.v72:210.1002/nme.1999](https://doi.org/10.1002/(ISSN)1097-020710.1002/nme.v72:210.1002/nme.1999).
- [47] Ł. Kaczmarczyk, M.M. Nezhad, C. Pearce, Three-dimensional brittle fracture: configurational-force-driven crack propagation, *Int. J. Numer. Meth. Eng.* 97 (7) (2014) 531–550, <https://doi.org/10.1002/nme.4603>.
- [48] S. Kim, H. Kim, S.Y. Kim, Configurational force on a dynamic dislocation with localized oscillation, *Int. J. Plast.* 136 (2021) 102814, <https://doi.org/10.1016/j.ijplas.2020.102814>.
- [49] R. Ballarini, G. Royer-Carfagni, A Newtonian interpretation of configurational forces on dislocations and cracks, *J. Mech. Phys. Solids* 95 (2016) 602–620, <https://doi.org/10.1016/j.jmps.2016.05.008>.
- [50] C. Kuhn, R. Lohkamp, F. Schneider, J.C. Aurich, R. Müller, Finite element computation of discrete configurational forces in crystal plasticity, *Int. J. Solids Struct.* 56–57 (2015) 62–77, <https://doi.org/10.1016/j.ijsolstr.2014.12.004>.
- [51] K. Özenc, G. Chinaryan, M. Kaliske, A configurational force approach to model the branching phenomenon in dynamic brittle fracture, *Eng. Fract. Mech.* 157 (2016) 26–42, <https://doi.org/10.1016/j.engfracmech.2016.02.017>.
- [52] L. Wang, W.M. Coombs, C.E. Augarde, M. Cortis, T.J. Charlton, M.J. Brown, J. Knappett, A. Brennan, C. Davidson, D. Richards, A. Blake, On the use of domain-based material point methods for problems involving large distortion, *Comput. Methods Appl. Mech. Eng.* 355 (2019) 1003–1025, <https://doi.org/10.1016/j.cma.2019.07.011>.
- [53] W.M. Coombs, C.E. Augarde, A.J. Brennan, M.J. Brown, T.J. Charlton, J. A. Knappett, Y. Ghaffari Motlagh, L. Wang, On Lagrangian mechanics and the implicit material point method for large deformation elasto-plasticity, *Comput. Methods Appl. Mech. Eng.* 358 (2020) 112622, <https://doi.org/10.1016/j.cma.2019.112622>.
- [54] T.J. Charlton, W.M. Coombs, C.E. Augarde, iGIMP: An implicit generalised interpolation material point method for large deformations, *Comput. Struct.* 190 (2017) 108–125, <https://doi.org/10.1016/j.compstruc.2017.05.004>.
- [55] W.M. Coombs, C.E. Augarde, AMPLE: a material point learning environment, *Adv. Eng. Softw.* 139 (2020) 102748, <https://doi.org/10.1016/j.advengsoft.2019.102748>.
- [56] C. Miehe, Comparison of two algorithms for the computation of fourth-order isotropic tensor functions, *Comput. Struct.* 66 (1) (1998) 37–43, [https://doi.org/10.1016/S0045-7949\(97\)00073-4](https://doi.org/10.1016/S0045-7949(97)00073-4).
- [57] A. de Vaucorbeil, V.P. Nguyen, S. Sinaie, J.Y. Wu, Material point method after 25 years: theory, implementation, and applications, *Adv. Appl. Mech.* (2020) 1–143, <https://doi.org/10.1016/bs.aams.2019.11.001>.
- [58] R. Zhou, Z. Li, J. Sun, Crack deflection and interface debonding in composite materials elucidated by the configuration force theory, *Compos. Part B Eng.* 42 (7) (2011) 1999–2003, <https://doi.org/10.1016/j.compositesb.2011.05.024>.
- [59] B. Näser, M. Kaliske, R. Müller, Material forces for inelastic models at large strains: application to fracture mechanics, *Comput. Mech.* 40 (6) (2007) 1005–1013, <https://doi.org/10.1007/s00466-007-0159-9>.
- [60] R. Mueller, D. Gross, G.A. Maugin, Use of material forces in adaptive finite element methods, *Comput. Mech.* 33 (6) (2004) 421–434, <https://doi.org/10.1007/s00466-003-0543-z>.
- [61] R. Denzer, F.J. Barth, P. Steinmann, Studies in elastic fracture mechanics based on the material force method, *Int. J. Numer. Meth. Eng.* 58 (12) (2003) 1817–1835, [https://doi.org/10.1002/\(ISSN\)1097-020710.1002/nme.v58:1210.1002/nme.834](https://doi.org/10.1002/(ISSN)1097-020710.1002/nme.v58:1210.1002/nme.834).
- [62] M. Fagerström, R. Larsson, Theory and numerics for finite deformation fracture modelling using strong discontinuities, *Int. J. Numer. Meth. Eng.* 66 (6) (2006) 911–948, [https://doi.org/10.1002/\(ISSN\)1097-020710.1002/nme.v66:610.1002/nme.1573](https://doi.org/10.1002/(ISSN)1097-020710.1002/nme.v66:610.1002/nme.1573).
- [63] A. Sadeghirad, R.M. Brannon, J. Burghardt, A convected particle domain interpolation technique to extend applicability of the material point method for problems involving massive deformations, *Int. J. Numer. Meth. Eng.* 86 (12) (2011) 1435–1456, <https://doi.org/10.1002/nme.3110>.
- [64] Ansys® Academic Research Mechanical, Release 18.1, Ansys Student Versions.
- [65] P.O. Bouchard, F. Bay, Y. Chastel, Numerical modelling of crack propagation: automatic remeshing and comparison of different criteria, *Comput. Methods Appl. Mech. Eng.* 192 (35-36) (2003) 3887–3908, [https://doi.org/10.1016/S0045-7825\(03\)00391-8](https://doi.org/10.1016/S0045-7825(03)00391-8).
- [66] A.R. Ingraffea, M. Grigoriu, (PDF) Probabilistic Fracture Mechanics: A Validation of Predictive Capability, 1990.
- [67] D. Azócar, M. Elgueta, M.C. Rivara, Automatic LEM crack propagation method based on local Lepp-Delaunay mesh refinement, *Adv. Eng. Softw.* 41 (2) (2010) 111–119, <https://doi.org/10.1016/j.advengsoft.2009.10.004>.